Fast and Dynamic Neighbourhood Energy Simulation by Coupling high-resolution CFD, Low-resolution –CFD and Building Energy Simulation Models

Abstract

Understanding of airflow in urban environment is essential in calculation of convections heat transfer coefficient (CHTC) from buildings' surfaces. However, microclimate effect is not presented in the current building energy simulation (BES) tools. Dynamic coupling of BES with computational fluid dynamics (CFD) techniques is a recommended strategy to include the urban airflow presence in building energy calculations. Nonetheless, this method is understood to be computationally intensive and unaffordable even in simplistic neighbourhood-scale scenarios.

This paper proposes a novel framework for integration of a high-resolution CFD model (CFD_f) into a coupled low-resolution CFD (CFD_c) and BES model. First, the CFD_f model (fine grids) operates as the off-line component in to provide boundary conditions to be used in CFD_c (coarse grids). Then, CFD_c and BES domains execute a fully dynamic external coupling to deliver an accurate energy simulation while achieving convergence for CHTC at exterior surfaces. A case study is performed for a simple neighbourhood environment on a typical hot day for a sheltered building scenario with cross night-purge cooling. The results highlight in a significant improvement of CHTC of the new dynamic coupling model with a runtime of about 195 times faster in comparison to the traditional coupling approaches.

Keywords: neighbour ventilation; CFD; microclimate modelling; building energy simulation; dynamic coupling

1. Introduction

Climate change and urbanization result in necessary actions in reducing building energy demand in urban areas. Unusual hot summer has been reported to be more frequent across the globe in the recent years with some to be even ranked among their highest temperature records [1]. The building cooling load is consequently raised especially in urban areas where demands of active cooling and air conditioning are dominantly high for providing indoor comfort [2, 3]. To conserve building energy demand, adequate usage of natural ventilation, such as night-purging, is known to be an effective strategy. To quantify the benefits of this strategy, tools are required to assess the energy demand of such buildings.

Building energy simulation (BES) approaches are developed with capabilities of modelling various building systems to predict the associated energy demands. There are many available commercial packages such as ENERGYPLUS, REVIT, ESP-r, and TRNSYS, which process the multi-zonal controls with nodal calculations, assuming the surrounding

environment to be neglected in the calculations [4]. Thus, these tools are rather very focused on indoor climate and systems rather than interactions with surrounding environment [5]. However, concerns have been raised against the simplified airflow modelling around the envelope surfaces that the neighbourhood effect in urban area [6] is either neglected or weakly represented by their embedded algorithms of the convective heat transfer coefficient (CHTC) for interior [7] and exterior surfaces [8]. These BES tools use empirical functions for convection at the building surfaces, which simplifies or ignores the urban microclimate. A simplified outdoor air model is reported to deliver energy information with error of 20 – 40 % [9, 10]. A potential way to improve the simulation is to introduce a powerful airflow-modelling component to be combined with BES. Computational fluid dynamics (CFD) technique is recommended as a high-resolution method widely being applied to solve microclimate airflow modelling, including the studies of pedestrian wind comfort [11], pollution dispersions [12], building energy [13-15], passive ventilation strategies [13, 16, 17], mechanical mechanisms [18], etc.

The coupling method, as been proved to improve the prediction of local convection by [19], can be related to both indoor and outdoor applications, however, they are mainly focused on modifying the airflow around the interior surfaces (e.g. [20] compared different coupling method and [21] proposed a controller for coupling process) and only a few on the externals (e.g. [22] undertook a case study for sealed buildings whilst the work of [23] was applied to naturally-ventilated buildings); almost a very limited are even developed for hybrid indoor-outdoor scenarios where natural ventilation is involved. For exterior surfaces, the limitation is due to the high computational burden, which is basically expended in the CFD domain, especially when neighbourhood effect is involved. In the cases of sealed building scenarios that only the mechanical ventilation is operating, when only outdoor environment is required to be considered in the CFD domain, a model of low-to-moderate size, but with appropriate configurations, may be adequate to deliver reliable results. For example, Zhang et al. combined BES with a valid CFD model consisting of only 13K cells for a simple city block with sealed commercial buildings and the results by coupling method showed a deviation up to 64% in local convection compared to that case simulated only by a stand-alone BES method [8]. One main challenge to assess natural ventilation in neighbourhood scale is that detailed descriptions of the site with a high-resolution CFD grid is necessary to be generated. For example, [16] and [24] employed CFD models with about 6.5M and 1M cells, respectively while [25] used cell size of 0.5 m for indoor spaces.

There are three ways to perform a CFD modelling of natural ventilation in buildings, including only consideration of the indoor domain [19] , consideration of both indoor and outdoor domains [23, 26] or performing multi-scale modelling (also called nesting technique) [27]. Most of the simulation studies use the second method that the model contains millions of cells, which make them impractical or feasible for employment in a fully dynamic coupling between CFD and BES to achieve a consistent solution between two models in each associated time-step. The study employing the nesting technique is rather limited. Mochida et al. [27] created two models, one (denoted as R1) was used to model the whole study

domain and the other one (denoted as R2) to cover only a near-field region around buildings. R2 was treated as a non-isothermal model to carry out precise calculation with boundary conditions extracted from the results of R1, which was processed isothermally with a less computational burden.

The challenge of coupling is thus understood as a reduction of the computational cost of the dynamic coupling without harm in results' quality. One approach is to expand the fully-dynamic coupling to a virtual coupling, which makes use of prediction tools (e.g. artificial neural network) to learn the relationships between environmental inputs and desired outputs. Some related researches can be found as [28, 29]. However, the collection process of training data for virtual tool development still requires significant computational resources. Therefore, the nesting technique becomes an attractive choice, especially when coupling into an iterative calculation.

This study aims to provide a framework of coupling BES with a coarse-resolution CFD (CFD_c) model and a fine-resolution CFD (CFD_f) model to provide higher potential for accurate energy modelling in urban areas. To investigate the performance of the developed framework, a night-purging natural ventilation in a sheltered commercial building scenario located in Los Angeles city is considered as the case study. Further to this introduction section, Section 2 explains the communication framework between CFD_f, CFD_c, and BES. Section 3 evaluates the performance of interface information exchange between two CFD domains. The detailed case study related to the proposed coupling method is also discussed in Section 3.

2. Methodology

2.1. Framework to integrate CFD_f – CFD_c - BES

Figure 1 shows the schematic of the proposed coupling CFD_f-CFD_c-BES method for energy assessment of buildings while the effect of natural ventilation is taken to the account. This framework is extended from a benchmark framework proposed by Zhang, et al. [8], which consists of two main components of CFD_c and BES, which are linked with a bespoke code. Now, an additional CFD_f component is included into the framework to enable the simulation of natural ventilation. Also, the bespoke code is modified as an interlink station between three domains and also the weather data, building and site information. While CFD_f model consists of a high-resolution grid for both indoor and outdoor domains, CFD_c consists of a coarse grid for only outdoor domain. Inflow and outflow boundaries should be inserted for the ventilation surfaces of the buildings in CFD_c as a deletion of its indoor part. The setups of these boundaries are obtained from the CFD_f simulation at the beginning. Therefore, the whole process can be divided into two stages of off-line preliminary simulation and online dynamic simulation.

Pre-simulation is implemented for a relatively short period of time (can be a few hours) before the simulation day so that the time lag effect in energy calculations is considered. As the results of CFD_f are fixed throughout the iterative dynamic stage, CFD_f domain only participate in an off-line stage. The embedded algorithm in BES domain calculate the initial

CHTC values in the preliminary stage for subsequent iterative calculations. When entering the dynamic simulation stage, convection control function of BES is then altered to 'user input' mode to receive updated results from CFD_c. Buildings are simulated using a fully dynamic approach that ensures a convergence between CFD_c and BES in exterior surfaces' convection for each time-step.

For the CFD_f component, the simulation period includes natural ventilation time (e.g. purging time including the night and the early morning when the space is unoccupied or relatively empty). The flow patterns that CFD_f passed to CFD_c include velocity and turbulence parameters at the opened ventilation surfaces. Moreover, the boundary conditions of CFD_c includes following aspects: (1) climatic conditions from BES weather data, (2) ventilating opening conditions determined by CFD_f and (3) other exterior surface conditions (e.g. surface temperatures) provided by BES. In this framework, building surface temperature (T_s) and CHTC are adopted as the exchange variables between CFD_c and BES. BES supplies CFD_c with the T_s and CFD_c feed the CHTC back to the bespoke code to update the CHTC schedule in BES. In general, both domains should achieve a similar convective heat flux (q_c'') with an acceptable small difference (e.g. less than 10^{-2} in this study) at the outdoor surfaces in every time-step before moving to the next one. The CFD_f and CFD_c simulations are performed by CFX and FLUENT packages of ANSYS 19.1©, respectively. BES modelling are employed by ENERGYPLUS 8.7© and the bespoke code was developed in MATLAB R18a©.

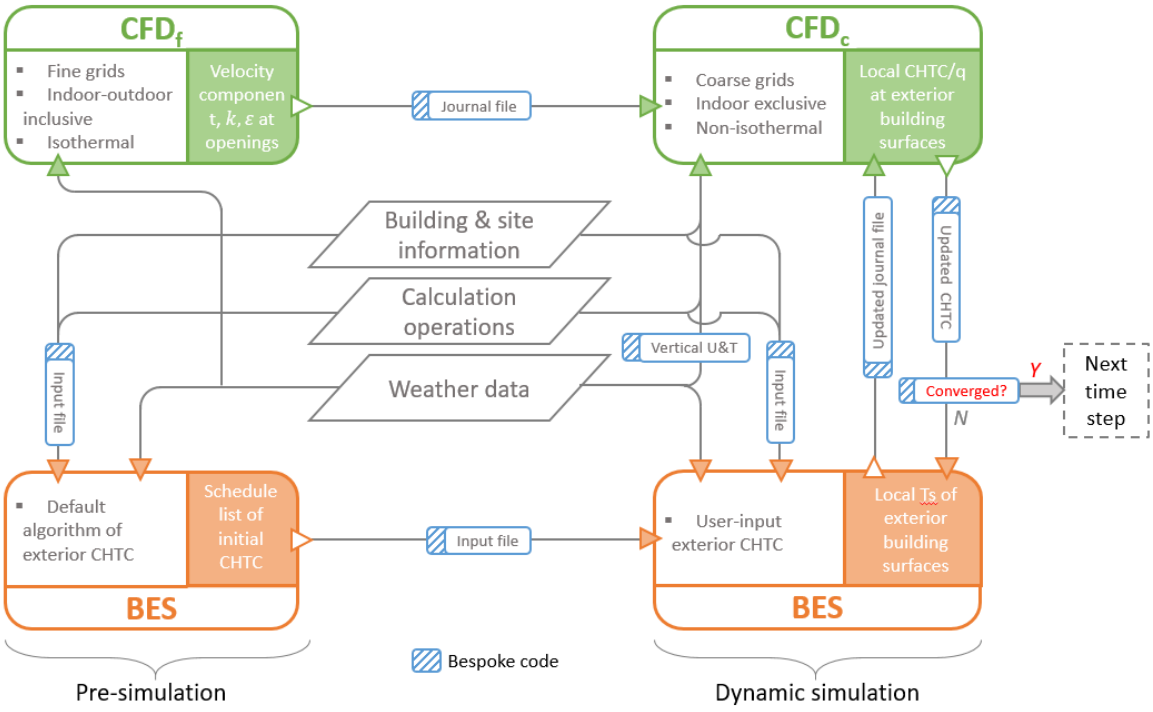

Figure 1 Framework of coupling CFD_f – CFD_c – BES for the exterior surface convection with the inclusion of natural ventilation

The principle of iterative calculation is to obtain an equivalent convective heat flux (q_c'') in both models. As the ENERGYPLUS calculate the local convective flux using a fixed air temperature ($T_{a,z}$, that is dependent on the elevation from the ground), a virtual CHTC (h_c^*) is

required to produce the convective heat gain as the same amount as that performed in the CFD_c domain. It should be noted that CFD_c uses the exact temperature of the surrounding flow ($T_{a,s}$). Thereby, during the iterative calculation, the h_c^* can be calculated by:

$$h_{c,i+1}^* = \frac{q''_{c,CFD_i}}{\left(T_{s,_i} - T_{a,z}\right)} \quad (1)$$

where i represents the current iteration index.

2.2. Case specification

A case study of simple city block is composed of nine cuboid buildings (10 m x 10 m x 10 m) in 3 x 3 array and the aspect ratio of each street canyon is unity as shown in *Figure 2*. Each building consists of three layers and the heights of the layers are set to be 3.4 m, 3.3 m and 3.3 m from the bottom to the top, respectively. There are windows placed on the south and north façades at each layer of the building. The window to wall ratio was kept as the same as a benchmark model in commercial use provided by the U.S. Department of Energy (DOE) [30].

Intense cooling is in demand in commercial buildings where insulation is regularly assigned and high internal heat gain released from occupants, lightings and other equipment. Therefore, the application of night-purging combined with mechanical ventilation provides a high potential in saving energy for commercial buildings as the space is unoccupied during the night. Thus, scenario of night-purging is assumed to investigate the use of cool night air to remove and absorb the stored heat from the building as a sink to be utilized for the following diurnal time [31]. The windows on top two layers were divided into two equal parts of W1 and W2 while W1s would be opened for night-purging. The simulation is processed for a typical hot day (September 25th) in Los Angeles U.S., including 12 hours of purging period (1 a.m. – 6 a.m. and 7 p.m. – 12 a.m.) and 12 hours of mechanical ventilation period during the working time.

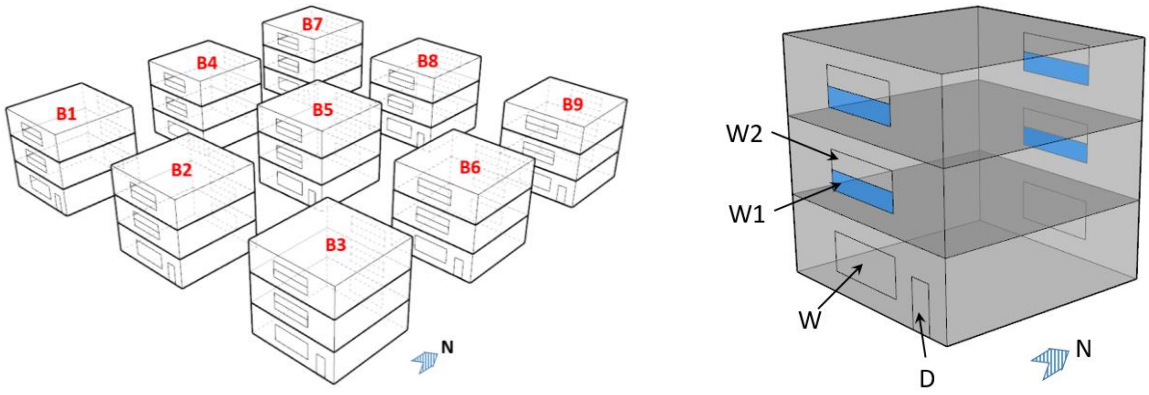

(a) (b)

Figure 2 Plot of a) nine cuboid commercial buildings and b) naming procedure of ventilation surfaces

2.3. Analytical model

The Reynolds Averaged Navier-Stokes (RANS) equations are applied as the governing equation for the airflow modelling:

$$\frac{\partial \rho}{\partial t} + \frac{\partial}{\partial x_j}\left(u_j\right) = 0 \tag{2}$$

$$\frac{\partial}{\partial t}\left(\rho u_j\right) + \rho u_j \frac{\partial}{\partial x_j}\left(u_i\right) = -\frac{\partial p}{\partial x_i} + \frac{\partial}{\partial x_j}\mu_{eff}\left[\left(\frac{\partial u_i}{\partial x_j} + \frac{\partial u_j}{\partial x_i}\right) - \frac{2}{3}\frac{\partial u_i}{\partial x_i}\bar{I}\right] + \rho\vec{g} \tag{3}$$

$$\frac{\partial}{\partial t}(\rho E) + \frac{\partial}{\partial x_i}u_i(\rho E + p) = \frac{\partial}{\partial x_j}\left[K_{eff}\frac{\partial T}{\partial x_j} - \sum_j h_j\bar{J}_j + \left(\bar{\bar{\tau}}_{eff}u_i\right)\right] + S_h \tag{4}$$

where t is the time, u is the mean flow velocity, ρ is the fluid density, p is the fluid pressure, $\rho\vec{g}$ is the term reflecting the gravitational force, and $\bar{I}$ is the unit tensor. E represents the total energy of the fluid ($E = h - \frac{p}{\rho} + 0.5u^2$), T is the temperature, h is the sensible enthalpy and $\bar{J}_j$ is the diffusion flux of the spices j, and the term involving the deviatoric stress tensor $\bar{\bar{\tau}}_{eff}$ represents the viscous heating. K_{eff} is the effective thermal conductivity and the μ_{eff} is the effective viscosity, which is defined as follows:

$$\mu_{eff} = \mu + \mu_t \tag{5}$$

where μ is the molecular viscosity and μ_t is the turbulence viscosity. The $k-\varepsilon$ model is employed in this study to solve the turbulence of the fluid. The relation of the turbulence viscosity to the turbulence kinetic energy (k) and dissipation rate (ε) is:

$$\mu_t = C_\mu \rho \frac{k^2}{\varepsilon} \tag{6}$$

where C_μ has a constant value.

The turbulence simulations in this study for CFD_c and CFD_f are set to be the standard $k-\varepsilon$ model or standard $k-\varepsilon$ model with modified closure coefficients obtained through a stochastic optimization process as stated in [32] (that the values were calibrated using the experimental data by [33]. The turbulence kinetic energy and dissipation rate are using the following transport equations:

$$\frac{\partial}{\partial t}(\rho k) + \frac{\partial}{\partial x_i}(\rho k u_i) = \frac{\partial}{\partial x_j}\left[\left(\mu + \frac{\mu_t}{\sigma_k}\right)\frac{\partial k}{\partial x_j}\right] + G_k + G_b - \rho\varepsilon \tag{7}$$

$$\frac{\partial}{\partial t}(\rho \varepsilon) + \frac{\partial}{\partial x_i}(\rho \varepsilon u_i) = \frac{\partial}{\partial x_j}\left[\left(\mu + \frac{\mu_t}{\sigma_\varepsilon}\right)\frac{\partial \varepsilon}{\partial x_j}\right] + C_{1\varepsilon}\frac{\varepsilon}{k}G_k - C_{2\varepsilon}\rho\frac{\varepsilon^2}{k} \tag{8}$$

where σ_k and σ_ε are the turbulent Prandtl number for k and ε, repectively. G_k and G_b are generated k terms by the mean velocity gradient and buoyancy, respectively. $C_{1\varepsilon}, C_{2\varepsilon}$ and $C_{3\varepsilon}$ are constant values. The default values assigned for CFDc's standard $k-\varepsilon$ model are as $C_\mu = 0.09$, $C_{1\varepsilon} = 1.44$, $C_{2\varepsilon} = 1.92$, $\sigma_k = 1.0$ and $\sigma_\varepsilon = 1.3$ [34]. However, the modified values used for CFDf modelling are $C_\mu = 0.141$, $C_{1\varepsilon} = 1.50$, $C_{2\varepsilon} = 3.20$, $\sigma_k = 1.0$ and $\sigma_\varepsilon = 0.294$ according to the results of calibrations. The definition of K_{eff} given by the standard $k-\varepsilon$ model is as below:

$$K_{eff} = K + \frac{c_p \mu_t}{Pr_t} \tag{9}$$

where K is the thermal conductivity, c_p is the thermal capacity of the fluid and Pr_t is the turbulent Prandtl number with a default value of 0.85.

For neutral ABL modelling, inlet boundary conditions for stream-wise velocity (u_z) is set based on a power-law profile in accordance with the presentation of wind speed in ENERGYPLUS:

$$u_z = u_{met}\left(\frac{\delta_{met}}{z_{met}}\right)^{\alpha_{met}}\left(\frac{z}{\delta}\right)^{\alpha} \tag{10}$$

where $z_{met} = 10$ m is the height of the velocity sensor at meteorological for stream-wise velocity u_{met} measurement, and $\delta_{\mathrm{met}} = 270$ m is the boundary layer thickness at the weather station. The velocity exponents for the weather station and the urban area around the target buildings are $\alpha_{met} = 0.14$ and $\alpha = 0.33$, respectively. The boundary layer thickness over the urban area around the buildings is $\delta = 460$ m. The vertical profiles for the k and ε were obtained using the following equations:

$$k_z = \frac{u'^2_{u,z} + u'^2_{v,z} + u'^2_{w,z}}{2} \cong \frac{3}{2}u'^2_{,z} = \frac{3}{2}(I_z u_z)^2 \tag{11}$$

$$\varepsilon_z = C_\mu^{1/2} k_z \frac{u_{ref}}{z_{ref}} \alpha \left(\frac{z}{z_{ref}}\right)^{\alpha-1} \tag{12}$$

where u'_z is the root mean square of the velocity fluctuations in stream-wise direction. C_μ is taken as 0.09 here. The subscript '*ref*' means the reference conditions, thereby, $u_{ref} = u_{met}$ and $z_{ref} = z_{met} = 10$ m in this study. I_z is the local turbulence intensity that can be calculated through the following equation:

$$I_z = 0.1\left(\frac{z}{\delta}\right)^{-\alpha-0.05} \tag{13}$$

where $\delta = 460$ m and $\alpha = 0.33$ for the urban area of this study.

The vertical temperature profiles ($T_{a,z}$,) at the inlet boundaries in the CFD domains were developed on the basis of the embedded equations in ENERGYPLUS to capture a similar pattern:

$$T_{a,z} = T_{a,z\,met} - \frac{E_r z_{met}}{(E_r + z_{met})} + \frac{E_r z}{(E_r + z)} \tag{14}$$

where L_a = -0.0065 K/m is the air temperature gradient throughout the troposphere, E_r = 6356000 m is the radius of the Earth. $T_{a,zmet}$ is the ambient temperature, which is normally measured by a sensor placed at z_{met} = 1.5 m above the ground.

In addition, the convective heat transfer coefficients of the exterior surfaces are determined by the embedded DOE-2 algorithm in ENERGYPLUS for this study. The DOE-2 algorithm calculated the exterior CHTC $h_{c,ext}$ using the following equations [35]:

$$h_{c,ext} = \begin{cases} \sqrt{{h_n}^2 + [a{u_z}^b]^2}, & for\ smooth\ surfaces\ (e.g.\ glass) \\ (1 - R_f)h_n + R_f\sqrt{{h_n}^2 + [a{u_z}^b]^2}, & for\ less\ smooth\ surfces \end{cases} \tag{15}$$

where R_f is the surface roughness multipliers, a and b are constants depending on whether the surface is leeward or windward, and h_n represents the natural component, which can be calculated through:

$$h_n = \begin{cases} \dfrac{9.482|\Delta T|^{1/3}}{7.283 - |cos\Sigma|}, & if \begin{cases} upward\ and\ \Delta T < 0 \\ downward\ and\ \Delta T > 0 \end{cases} \\ \dfrac{1.810|\Delta T|^{1/3}}{1.382 + |cos\Sigma|}, & if \begin{cases} upward\ and\ \Delta T > 0 \\ downward\ and\ \Delta T < 0 \end{cases} \end{cases} \tag{16}$$

where Σ is the surface tilt from the horizontal, and ΔT is the temperature difference between the exterior surface and the local ambient air ($\Delta T = T_{air,z} - T_s$).

2.4. CFD domains

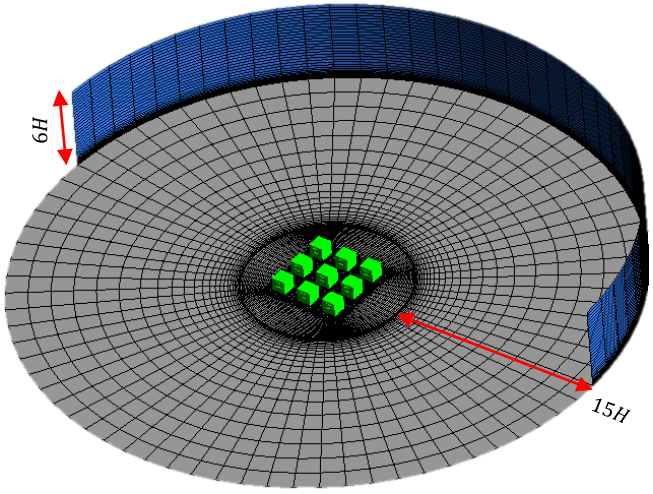

Figure 3 Cylindrical domain for the microclimate modelling

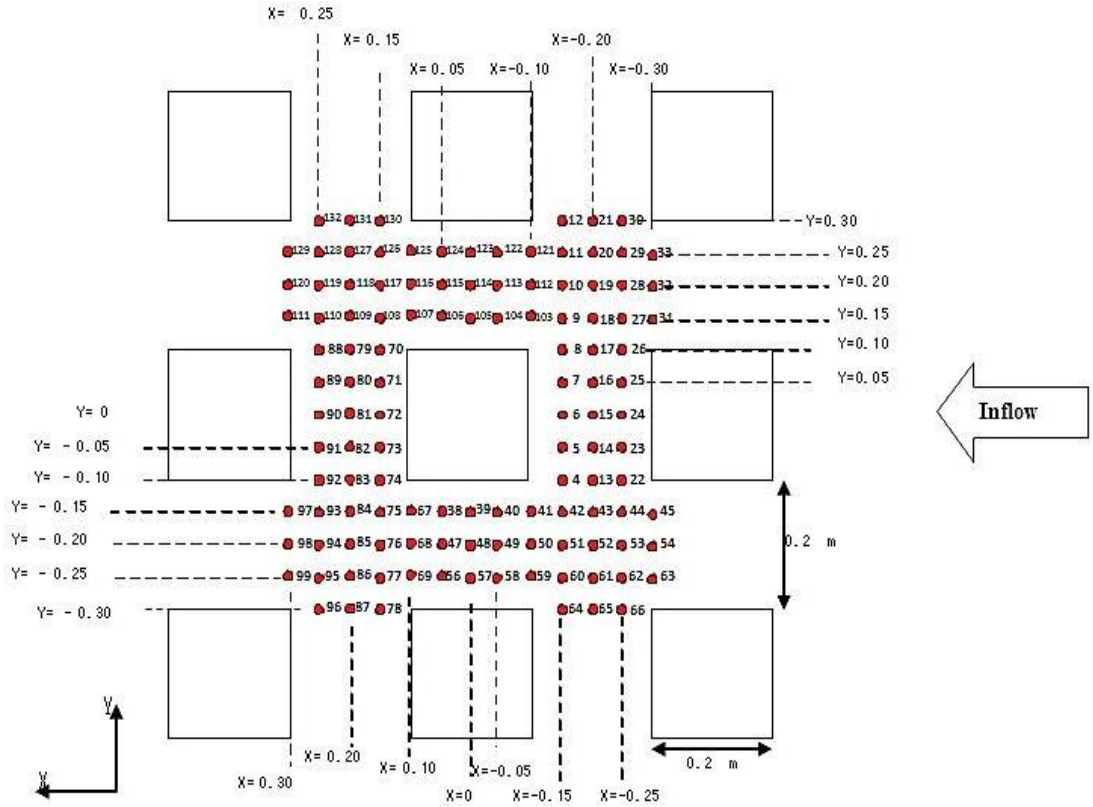

Figure 4 (a) Distribution of 120 test points (Source: Architecture Institution of Japan, Validation Benchmark Tests Case C [36]) and (b) Plot of normalized velocity versus normalized experimental measurements for CFD_c validation

A cylindrical computational domain (see *Figure 3*) was employed in accordance with the recommendations in [37, 38]. Both CFD_f and CFD_c domains were created and validated against measurements of wind tunnel experiments conducted in Niigata Institute of

Technology [33] and Architectural Institute of Japan [36], respectively. The prediction error of the airflow rate was found as 7% for the calibrated configurations of CFD_f with the proposed coefficients for the modified $k-\varepsilon$ model. More details of CFD_f model's validation are found in Ref. [32]. The final CFD_f model for the case study contains approximately 7.5 million cells. The CFD_c model was developed from the one reported in study [8] with only 130k cells, in which the mean prediction error of the velocity at 120 points was found about 13% (shown in *Figure 4a*); all the points are placed at 0.02 m above the ground. The mean prediction error of local velocities at those points placed in the first layer (with a distance of 0.15 m from the B5 facades) around the target building was approximately 10% (with a median value around 4%). *Figure 4b* displays the comparison of calculated local velocity and experimental measurements on these 120 points. The hit rate of CFD_c was calculated as approximately 0.79, higher than the recommended level (0.66) by COST guidelines [39]. It has been found that CFD_c with the standard $k-\varepsilon$ model shows a better representation of airflow in CFD_f than that of with the modified $k-\varepsilon$ model. CFD_c is designed to have merely indoor environment, however, with the capability of representing the microclimate around naturally ventilated buildings. Therefore, to capture the patterns of the flow entering the windows (Af_1) and the flow leaving the windows (Af_2), the flow information obtained in CFD_f is passed to CFD_c to define the boundaries (see in ***Error! Reference source not found.***). It should be noted that in CFD_c if the flow direction is pointed towards the interior space, then the window boundary should be defined as outflow (Af_1) whilst inflow boundary is assigned to the windows, releasing air to the exteriors (Af_2). The boundaries in CFD_c can be defined with velocity components ($u_{(x,y,z)}$), pressure (p) or math flowrate ($\dot{M}$) with k and ε. In this study, the transferred parameters are velocity components, k and ε. The selection process is described in Section 3.1.

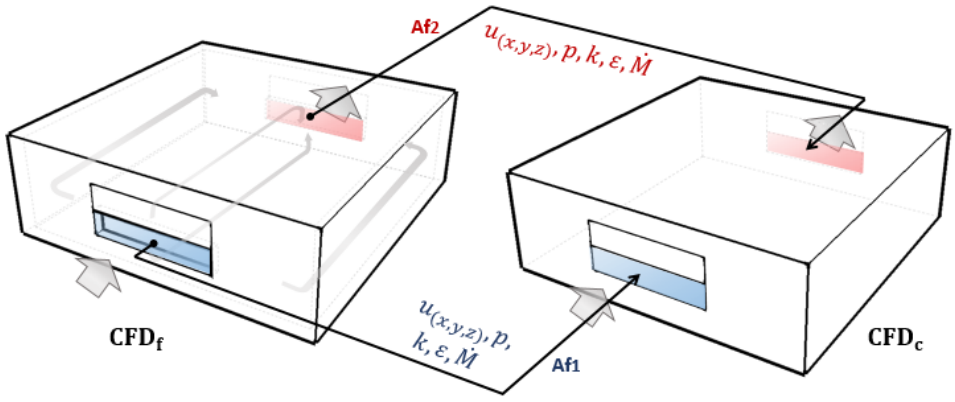

Figure 5 Flow information transfer from CFD_f to CFD_c

Table 1 elaborates the boundary conditions assigned for the CFD_f and CFD_c domains. SIMPLE algorithm was used to solve the RANS equations for CFD_c and the default embedded algorithm in CFD_f is the COUPLED algorithm. All the equations were solved through the second order transient schemes. The standard and scalable wall treatments were employed for CFD_c and CFD_f domains, respectively, to match their requirements of solving the boundary layers according to the sizes of their first layer cells.

Table 1 Boundary conditions of CFD_f and CFD_c domains

Boundary	Type	CFD_f	CFD_c
Ground	Wall	No-slip Constant temperature, *Tg	
Building surfaces	Wall	No-slip Constant Temperature, Ts from BES (fixed)	No-slip Constant Temperature, Ts from BES (updated)
Other walls	Wall	No-slip, Smooth wall Adiabatic	
Sky	Symmetry		
Inlet (Cylinder)	Velocity inlet	Components specified velocity method: Velocity components, U (x) and V(y) from the vertical profile, W(z) = 0 k and ε from the vertical profile Temperature from the vertical profile	
Outflow (Cylinder)	Pressure outlet	Gauge pressure = 0 pa k and ε from the vertical profile Temperature from the vertical profile	Average static pressure = 0 pa
Ventilating windows	Velocity inlet/outlet	-	Components specified velocity method: Velocity components x, y and z from CFD_f

*T_g is the ground temperature from weather data.

3. Results & Discussion

3.1. Boundary type selection

Velocity boundary is employed in CFD_c in order to develop the same or similar features of ventilation surfaces as those performed in CFD_f. To achieve that, the velocity of ventilating surfaces is specified using three-dimensional components obtained in CFD_f. The root mean square error (RMSE) in terms of the pressure coefficient (c_p), the flow velocity (u), the pressure (p) and the mass flow rate ($\dot{M}$), at all ventilating surfaces by the CFD_c comparing to CFD_f is investigated. It is found that the representation of pressure coefficient and pressure is less accurate than the other two variables, but still within an acceptable region (their RMSE are 0.658 and 0.655, respectively). The employed velocity boundaries provide a highly accurate scene restoration in terms of velocity and mass flow rate with RMSE of 0.104 and 0, respectively. 58 test lines (34 vertical and 24 horizontal lines) are created inside the street canyons to assess the accuracy of CFD_c in modelling the vertical and horizontal flow patterns. The velocity boundary is selected as considering its overall strength in representations of flow characteristics at opening surfaces and street canyon flows as well as the stability and speed of convergence. More details of boundary type analysis and the comparison of the flow characteristics' modelling by CFD_f-BES and CFD_f-CFD_c-BES methods have been reported in Ref. [40]. *Figure 6* shows RMSE of the normalized local velocity of these lines over the meteorological wind speed.

Although the accuracy is compromised by using CFD_c instead of CFD_f, the coupling CFD_f – CFD_c has benefits the run time and computational cost considerably. In the same isothermal scenario, the simulation of CFD_c only takes 1/28 of the runtime associated to CFD_f. The benefits of runtime conservation are even more obvious when non-isothermal conditions are considered. As seen in *Table 2*, in the first hour of the test day for instance, the proposed CFD_f–CFD_c–BES takes considerably less time to complete one iteration compared to the CFD_f–BES method (approximately 1/70 in general). Moreover, it can be found that the proposed coupling method performed its advantages in a faster convergence while it only takes three iterations to converge comparing to 8 iterations by the conventional method. Therefore, the total saving in runtime becomes significant as it can be seen that the simulation using the proposed methods takes merely 1/195 of the runtime of CFD_f -BES.

Figure 7 shows the plot of residuals of CHTC by CFD domains between two continuous iterative calculations during the first hour of the day. The residuals achieved by the proposed CFD_f-CFD_c-BES method and conventional method are 0.0012 and 8.94, respectively. The proposed method approaches smoothly and stably to its convergence with a lower value. In contrast, the conventional CFD_f–BES method is found to struggle to reach its convergence and fluctuate around relatively high level of residuals. This can be attributed to the intense calculation difficulty in processing high-resolution grids with complex environments. The error due to the poor convergence of CFD_f–BES method may be transmitted and accumulated along the iterations and cause concerns in the accuracy of the whole coupling method.

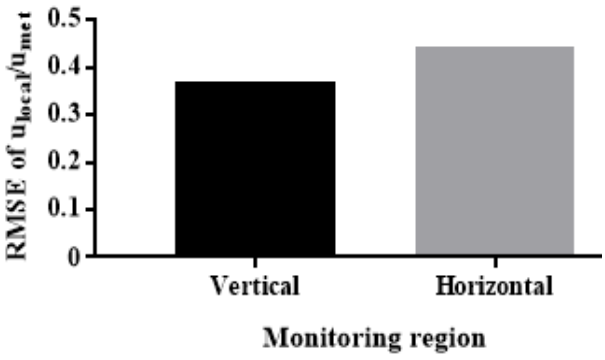

Figure 6 RMSE of the normalised velocity in different monitoring regions

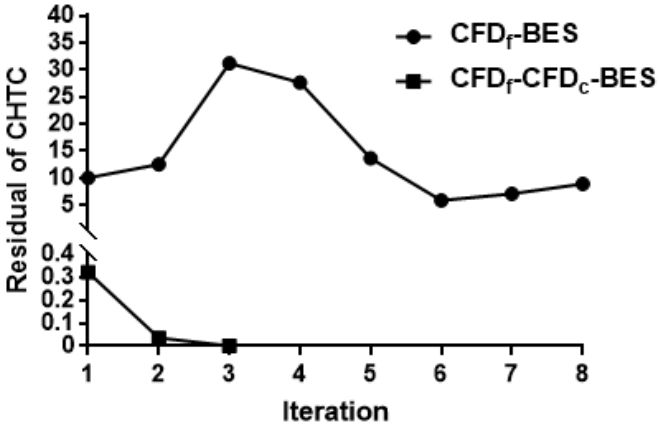

Figure 7 Plot of residuals of CHTC for every iterative calculation by CFD_f-BES and CFD_f-CFD_c-BES methods during the 1st hour of the test day

Table 2 Runtime of every iterative calculation by CFD_f-BES and CFD_f-CFD_c-BES methods for the 1st hour of the test day

Iteration	CFD_f-BES	CFD_f-CFD_c-BES
iter-1	12:06:04	00:10:19
iter-2	11:14:34	00:10:26
iter-3	14:07:57	00:11:19
iter-4	11:53:02	Converged

iter-5	11:35:22	
iter-6	12:55:11	
iter-7	12:21:23	
iter-8	12:38:40	
	Converged	
Total Runtime	98:52:14	0:32:04

3.2. Comparison of stand-alone BES and coupling method

Convergence between CFD_c and BES is achieved to a criterion of 0.01. However, if it is struggling to reach such criterion within 10 iterations, it would be extended to maintain the efficiency, as 0.1 in this study. *Figure 8* shows the number of iterations taken to get reliable results in each tested time-step.

Figure 9 shows the difference of zonal temperatures of the building in the centre of the community (see B5 in *Figure 2*) provided by the proposed coupling and the stand-alone BES methods. The figure displays the results for all purging hours (1 a.m. – 6 a.m. and 7 p.m. – 12 p.m.) and two hours (7 a.m. and 8 a.m.) after the first purging period when the difference in cooling simulation was still taking effect with the time lag. As for the other working hours, except the first two hours after the purging period, the temperature difference between the results of two methods was negligible as the zones are under the control of HVAC system. The positive values indicates that the zonal temperatures are underestimated by DOE-2 algorithm. The magnitude of temperature difference during the first purging period (1 a.m. – 6 a.m.) is much higher than that in the second purging period (7 p.m. – 12 p.m.). As looking into the weather data, from 1 a.m. – 6 a.m., the approaching winds are from the north side; however, the approaching winds are from the south side during 7 p.m. – 12 p.m. Thereby, the accuracy of the DOE-2 algorithm is observed to be sensitive to the wind direction.

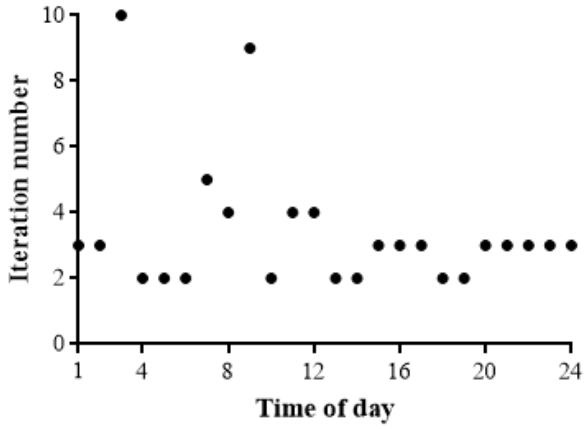

Figure 8 Iteration numbers to achieve convergence

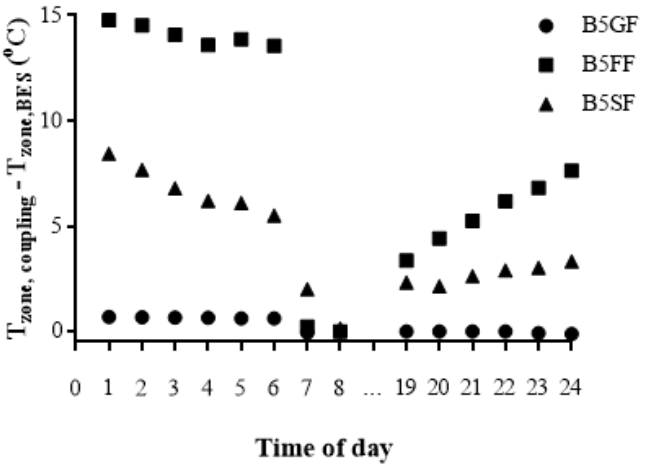

Figure 9 Difference of Building #5's zone temperature computed by the coupling and stand-alone BES methods

From 1 a.m. to 6 a.m. and from 7 p.m. to 12 p.m., the top two floors are naturally ventilated whilst the ground floor (GF) is almost isolated from the environment. Since the temperature difference on the GF is only dependent on the update of CHTC, it is supposed to be lower than the other two temperature differences and the results of the simulation approves that. Moreover, during the purging hours, the temperature difference on the first floor (FF) is found to be the highest. Even if the height difference is contributing, but its influence is small thereby it is taken aside. Taking FF as the benchmark (e.g. from 1 a.m. – 6 a.m.), the values of the second floor (SF) under both ventilation and convection conditions are approximately twice to three times of those of FF (as seen from *Figure 9*). Large differences are found between the GF and the top two floors. This means that the ventilation has played a larger share of heat exchange comparing to the convection part. The biggest difference of SF to FF is that SF contains the roof surface, which implies that the coupling method to update CHTC on the roof surface has compensated part of the influence of the inclusion of the natural ventilation as it has a great influence on the roof surface temperature. This finding is confirmed by the fact that the largest deviation occurs at the second floor (SF) at the 7th hours of the day when natural ventilation is deactivated and the temperature difference on GF and first floor (FF) is minimal as shown in *Figure 9*. It can also be drawn that the BES only method has overestimated the volume of the natural ventilation.

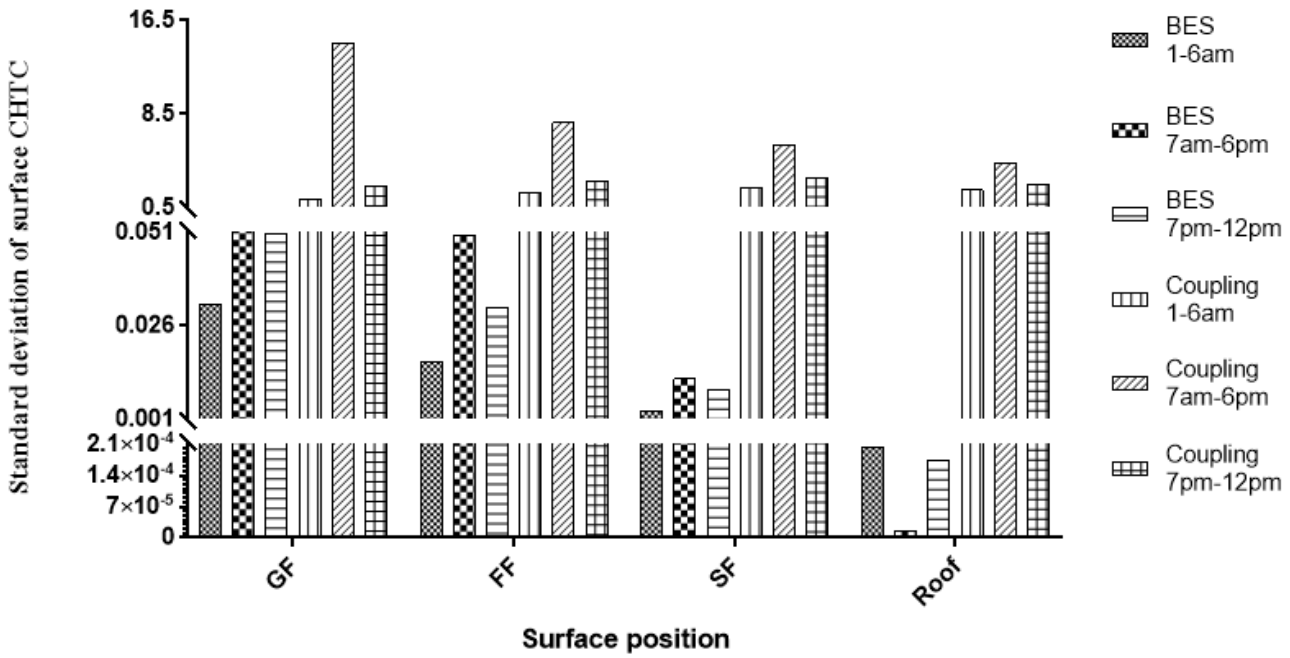

Figure 10 Standard deviation of surface CHTC by stand-alone BES and dynamic coupling method

ENERGYPLUS, or other BES tool, considers the effect of wind directions simply by dividing the walls into two categories of windward or leeward (as seen from *Equation 15*). Thus, the difference between building and building is systematically ignored by the embedded CHTC algorithms of the BES tools. The advantage of coupling CFD simulations is therefore to significantly improve the airflow modelling and then improves the representation of the

surrounding environment. *Figure 10* clearly displays the standard deviation of CHTC at the exterior surfaces (categorized by different altitudes) in the neighbourhood environment. The standard deviations obtained by stand-alone BES are found fairly small, that the highest value is approximately 0.05 during the natural-ventilating time, which means that the negligible neighbourhood effect is considered. In contrast, the proposed dynamic coupling method has fully reflected the neighbourhood effect as can be explored from the obvious higher standard deviation (magnified by in average by 28K times), especially at the roof surfaces. During the night-purging hours, the standard deviation of the roofs' CHTC by stand-alone BES is approximately 1.9E-04 whilst it is 2.2E+00 as obtained by the coupling method. In the working hours, this value is found as 1.4E-05 by stand-alone BES and 4.4E+00 by the coupling method, respectively.

Figure 11 demonstrates the cooling effect of the associated night purging strategy. The comparison is provided between the cases with mechanical ventilation by stand-alone BES and coupling CFD-BES methods and the cases with night-purge cooling with day-time mechanical ventilation simulated by stand-alone BES and the proposed integrating methods. The difference between two modelling methods for the mechanical ventilations is due to the enhanced representation of the neighbourhood effect by the coupling approach. The impact of night-time natural ventilation on conservation of daytime cooling energy can be reflected by comparing the values of CFD-BES Mechanical with those of CFD_f-CFD_c-BES Night purging ones, or the values of BES Mechanical with those of BES Night-purging ones. As it can be found from the figure, there is an obvious reduction of cooling load from the cases with mechanical ventilation to those with night-purge cooling with the corresponding method, respectively. This approves the advantages of night-purging strategy in saving cooling energy. The reduction of cooling load by the night-purging is observed to be smaller by the coupling methods than that of the BES only method. It can be explained that the indoor spaces are under warmer conditions by using the proposed coupling method though the working hours are simulated without influence of the natural ventilation. The difference of boundary conditions due to the time-lag effect has also been considered within the convection calculations. Larger discrepancy can be discovered during earlier hours (when both pre-cooling of night-purging and modification of CHTC are taking effect) of day-time period for scenarios with night-purging scenarios are modelled by two different methods. The discrepancy between two values (BES Night-purging and CFD_f-CFD_c-BES Night-purging) is then reaching to a smaller value across marching through the time and also in final few hours of the daytime; it eventually ends at a value similar to the gap between BES Mechanical and CFD-BES Mechanical. The total daily cooling loads of the community under night-purging scenarios by stand-alone BES and coupling CFD_f-CFD_c-BES methods are caudated as 1,466.8 kWh and 2,033.8 kWh, respectively. In addition, the average standard deviation of the cooling loads of nines buildings is 1.79 by the BES only method compared to 2.01 calculated by the proposed coupling method.

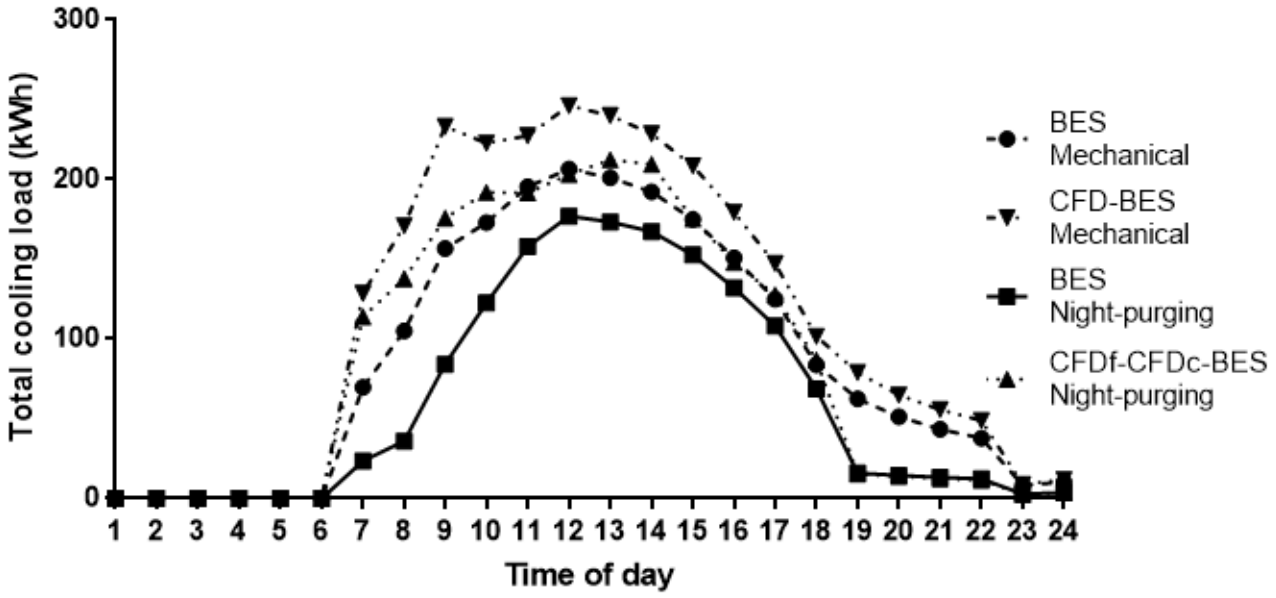

Figure 11 Total cooling load of the community throughout the test day

4. Conclusions

Coupling BES and CFD tools to improve convective heat transfer modelling has been proposed in many studies. However, when the method is applied to the cases of natural ventilation (for example in night-purge cooing), issues of heavy computational load and long runtime are raised, which is critically due to the difficulties in processing dynamic calculations in the CFD domain. On the other hand, to resolve the details related to the natural ventilation in buildings, high-resolution grids are required to capture airflow in both indoor and outdoor environment. Therefore, a fully dynamic framework of coupling of CFD_f, CFD_c and BES is developed to model the naturally ventilated buildings in urban areas. The framework aims to enhance exterior convection predictions with improving runtime efficiency.

The concept of coupling of CFD_f and CFD_c is found to be feasible with obtaining acceptable velocity and mass flow rate fields in both models. The advantage in conservation of runtime is considerable as it only takes less than 1/28 of the required time by replacing CFD_f with CFD_c model in each simulation. When considering the non-isothermal scenarios, the strength of the proposed CFD_f-CFD_c-BES method becomes more obvious as it takes merely 1/195 of runtime of that executed by CFD_f-BES method to complete the dynamic iterative modelling.

The coupling method is found to be effective in improving the inclusion of neighbourhood effect in energy modelling. The roof surfaces are found as the place where the effect has been reflected strongest during the purging hours with a standard deviation of 1.7E+00 in comparison to 2.1E-04 found by stand-alone BES method. Furthermore, the standard deviations of cooling load of nine buildings are 1.79 and 2.01 by stand-alone BES and the coupling methods, respectively. The future work will focus toward improvement of a long-term application of the proposed framework.

Acknowledgements

The authors would like to acknowledge the financial support from the Faculty of Engineering of The University of Nottingham, UK.

References

1. NOAA National Centers for Environmental information. *Climate at a Glance: Global Time Series*. 2019 July 2019 [cited 2019 August 6]; Available from: https://www.ncdc.noaa.gov/cag/global/time-series/globe/land_ocean/ytd/7/1880-2018.
2. International Energy Agency, *The Future of Cooling: Opportunities for energy-efficient air conditioning*. 2018, OECD, IEA. p. 92.
3. Watkins, R., et al., *The London heat island: results from summertime monitoring.* Building Services Engineering Research and Technology, 2002. **23**(2): p. 97-106.
4. Negrão, C.O.R., *Integration of computational fluid dynamics with building thermal and mass flow simulation.* Energy and Buildings, 1998. **27**(2): p. 155-165.
5. Zhai, Z. and Q.Y. Chen, *Solution characters of iterative coupling between energy simulation and CFD programs.* Energy and buildings, 2003. **35**(5): p. 493-505.
6. Mirzaei, P.A., et al., *Urban neighborhood characteristics influence on a building indoor environment.* Sustainable Cities and Society, 2015. **19**: p. 403-413.
7. Zhai, Z., et al., *Strategies for coupling energy simulation and computational fluid dynamics programs*. 2001.
8. Zhang, R., P.A. Mirzaei, and B. Jones, *Development of a dynamic external CFD and BES coupling framework for application of urban neighbourhoods energy modelling.* Building and Environment, 2018. **146**: p. 37-49.
9. Buchanan, C., *CFD simulation of infiltration heat recovery.* Lawrence Berkeley National Laboratory, 2011.
10. Emmel, M.G., M.O. Abadie, and N. Mendes, *New external convective heat transfer coefficient correlations for isolated low-rise buildings.* Energy and Buildings, 2007. **39**(3): p. 335-342.
11. Mirzaei, P.A. and F. Haghighat, *A novel approach to enhance outdoor air quality: Pedestrian ventilation system.* Building and Environment, 2010. **45**(7): p. 1582-1593.
12. Mirzaei, P.A. and F. Haghighat, *Pollution removal effectiveness of the pedestrian ventilation system.* Journal of Wind Engineering and Industrial Aerodynamics, 2011. **99**(1): p. 46-58.
13. Shirzadi, M., P.A. Mirzaei, and M. Naghashzadegan, *Development of an adaptive discharge coefficient to improve the accuracy of cross-ventilation airflow calculation in building energy simulation tools.* Building and Environment, 2018. **127**(Supplement C): p. 277-290.
14. Allegrini, J., V. Dorer, and J. Carmeliet, *Coupled CFD, radiation and building energy model for studying heat fluxes in an urban environment with generic building configurations.* Sustainable Cities and Society, 2015. **19**: p. 385-394.
15. Yamamoto, T., et al., *Fundamental study of coupling methods between energy simulation and CFD.* Energy and Buildings, 2018. **159**: p. 587-599.
16. Shirzadi, M., M. Naghashzadegan, and P. A. Mirzaei, *Improving the CFD modelling of cross-ventilation in highly-packed urban areas.* Sustainable Cities and Society, 2018. **37**: p. 451-465.
17. Gilani, S., H. Montazeri, and B. Blocken, *CFD simulation of stratified indoor environment in displacement ventilation: Validation and sensitivity analysis.* Building and Environment, 2016. **95**(Supplement C): p. 299-313.
18. Kuznik, F., G. Rusaouën, and J. Brau, *Experimental and numerical study of a full scale ventilated enclosure: Comparison of four two equations closure turbulence models.* Building and Environment, 2007. **42**(3): p. 1043-1053.
19. Zhai, Z.J. and Q.Y. Chen, *Performance of coupled building energy and CFD simulations.* Energy and Buildings, 2005. **37**(4): p. 333-344.
20. Djunaedy, E., J. Hensen, and M. Loomans, *External coupling between CFD and energy simulation: implementation and validation.* ASHRAE Transactions, 2005. **111**(1): p. 612-624.
21. Beausoleil-Morrison, I., *The adaptive conflation of computational fluid dynamics with whole-building thermal simulation.* Energy and Buildings, 2002. **34**(9): p. 857-871.

22. Yi, Y.K. and N. Feng, *Dynamic integration between building energy simulation (BES) and computational fluid dynamics (CFD) simulation for building exterior surface.* Building Simulation, 2013. **6**(3): p. 297-308.
23. Zhang, R., et al., *Coupled EnergyPlus and computational fluid dynamics simulation for natural ventilation.* Building and Environment, 2013. **68**: p. 100-113.
24. Kim, H., et al. *Application of coupled simulation between bes-cfd for naturally ventilated residential buildings*. in *13th Conference of the International Building Performance Simulation Association, BS 2013*. 2013.
25. Carrilho da Graça, G., et al., *Simulation of wind-driven ventilative cooling systems for an apartment building in Beijing and Shanghai.* Energy and Buildings, 2002. **34**(1): p. 1-11.
26. Wang, L. and N.H. Wong, *Coupled simulations for naturally ventilated rooms between building simulation (BS) and computational fluid dynamics (CFD) for better prediction of indoor thermal environment.* Building and Environment, 2009. **44**(1): p. 95-112.
27. Mochida, A., et al., *Total analysis of cooling effects of cross-ventilation affected by microclimate around a building.* Solar Energy, 2006. **80**(4): p. 371-382.
28. Ren, C. and S.-J. Cao, *Development and application of linear ventilation and temperature models for indoor environmental prediction and HVAC systems control.* Sustainable Cities and Society, 2019. **51**: p. 101673.
29. Ren, C. and S.-J. Cao, *Implementation and visualization of artificial intelligent ventilation control system using fast prediction models and limited monitoring data.* Sustainable Cities and Society, 2020. **52**: p. 101860.
30. Deru, M., et al., *US Department of Energy commercial reference building models of the national building stock.* 2011.
31. Iyengar, K., *Sustainable Architectural Design: An Overview*. 2015: Taylor & Francis.
32. Shirzadi, M., et al., *Modelling enhancement of cross-ventilation in sheltered buildings using stochastic optimization.* International Journal of Heat and Mass Transfer, 2018. **118**(Supplement C): p. 758-772.
33. Tominaga, Y. and B. Blocken, *Wind tunnel experiments on cross-ventilation flow of a generic building with contaminant dispersion in unsheltered and sheltered conditions.* Building and Environment, 2015. **92**: p. 452-461.
34. Launder, B.E. and D.B. Spalding, *The numerical computation of turbulent flows.* Computer Methods in Applied Mechanics and Engineering, 1974. **3**(2): p. 269-289.
35. Department of Energy U.S., *EnergyPlus Engineering Reference*. 2016.
36. Architectural Institute of Japan, *Guidebook for practical applications of CFD to pedestrian wind environment around buildings*. Architectural Institute of Jpan.
37. Mirzaei, P.A. and J. Carmeliet, *Dynamical computational fluid dynamics modeling of the stochastic wind for application of urban studies.* Building and Environment, 2013. **70**: p. 161-170.
38. Tominaga, Y., et al., *AIJ guidelines for practical applications of CFD to pedestrian wind environment around buildings.* Journal of Wind Engineering and Industrial Aerodynamics, 2008. **96**(10–11): p. 1749-1761.
39. Schatzmann, M., H.R. Olesen, and J. Franke, *COST 732 model evaluation case studies: approach and results*. 2010: COST Office.
40. Zhang, R. and P.A. Mirzaei, *CFD-CFD coupling: A novel method to develop a fast urban microclimate model.* Journal of Building Physics. **0**(0): p. 1744259120935921.